electronic reprint

Journal of
Synchrotron Radiation
ISSN 0909-0495
Editors: **Å. Kvick, D. M. Mills and T. Ohta**

Coherent X-ray scattering and lensless imaging at the European XFEL Facility

I. A. Vartanyants, I. K. Robinson, I. McNulty, C. David, P. Wochner and Th. Tschentscher

Copyright © International Union of Crystallography

Author(s) of this paper may load this reprint on their own web site or institutional repository provided that this cover page is retained. Republication of this article or its storage in electronic databases other than as specified above is not permitted without prior permission in writing from the IUCr.

For further information see http://journals.iucr.org/services/authorrights.html

Journal of
Synchrotron Radiation
ISSN 0909-0495

Received 2 May 2007
Accepted 31 July 2007

Coherent X-ray scattering and lensless imaging at the European XFEL Facility

I. A. Vartanyants,[a]* I. K. Robinson,[b] I. McNulty,[c] C. David,[d] P. Wochner[e] and Th. Tschentscher[a]

[a]HASYLAB at DESY, Notkestrasse 85, 22607 Hamburg, Germany, [b]London Centre for Nanotechnology, Department of Physics and Astronomy, University College, London WC1E 6BT, UK, [c]Advanced Photon Source, Argonne National Laboratory, 9700 South Cass Avenue, Argonne, IL 60439, USA, [d]Paul Scherrer Insitut, CH-5232 Villigen PSI, Switzerland, and [e]Max-Planck-Insitut für Metallforschung, Heisenbergstrasse 3, D-70569 Stuttgart, Germany.
E-mail: ivan.vartaniants@desy.de

Coherent X-ray diffraction imaging is a rapidly advancing form of lensless microscopy. The phase information of the diffraction pattern is embedded in a sufficiently sampled coherent diffraction pattern. Using advanced computational methods, this diffraction pattern can be inverted to produce an image of a sample with diffraction-limited resolution. It is attractive to use high-power coherent X-ray beams produced by future X-ray free-electron lasers for imaging nanoscale condensed matter, materials and biological samples. Here, the scientific case, requirements and the possible realisation of the coherent X-ray diffraction imaging beamlines at the European XFEL Facility are presented.

© 2007 International Union of Crystallography
Printed in Singapore – all rights reserved

Keywords: X-ray free-electron laser; coherent X-ray diffraction imaging; phase retrieval.

1. Introduction

Coherent X-ray diffraction imaging (CXDI) is a rapidly advancing form of lensless microscopy that was opened up by the realisation that oversampled diffraction patterns can be inverted to obtain real-space images. The possibility was first pointed out by Sayre (1952) but not demonstrated until 1999 by Miao *et al.* (1999). The phase information of the diffraction pattern, which is lost in its recording, is embedded in a sufficiently sampled coherent diffraction pattern, because this is intimately related to the Fourier transform of the object under investigation. The inversion of diffraction back to an image has been proven to be unique in two or higher dimensions, except for 'pathological' cases of internal symmetry of the object or its diffraction pattern (Bates, 1982; Hayes, 1982). Computational methods for performing the inversion, under very general constraints (*e.g.* for finite support of a sample, positivity of electron density *etc.*), are under active development; they are often based on the iterative hybrid input–output method introduced in the 1980s by Fienup (1982).

Lensless imaging using coherent X-rays is an attractive alternative to electron microscopy because of better penetration of the electromagnetic waves in materials of interest; also, multiple scattering effects can be neglected, so that the first Born approximation (or, in other words, kinematical scattering) can be safely used. In many cases X-rays are less damaging to the sample than electrons and, in either case, the collection of a diffraction pattern is inherently more efficient than the use of lenses (Henderson, 1995). If the diffraction can be reliably inverted by computation, the method could be routinely used to reveal the structure of materials on the nanometer scale, far beyond the resolution of the traditional light microscope. The holographic method of combining a reference wave is an alternative way to perform the inversion (Eisebitt *et al.*, 2004).

X-ray free-electron lasers (XFELs) based on self-amplified spontaneous emission (SASE) provide the best opportunity for the future development of CXDI methods and its applications to material science and biology. With the LCLS (Linac Coherent Light Source) in the USA (Arthur *et al.*, 2002), SCSS (Spring-8 Compact SASE Source) in Japan (Tanaka & Shintake, 2005) and the European XFEL Facility in Germany (Altarelli *et al.*, 2006), several hard X-ray FEL sources are under construction or in the final approval stage. Unique properties of hard X-ray FEL radiation are its high peak brilliance (corresponding to 10^{12} photons in a single pulse) and the ultrashort pulse duration of 100 fs. These sources allow us to consider applications of CXDI to structural analysis of nanometer-scale particles, inaccessible using third-generation undulator sources. Lensless imaging is particularly well suited to the unique capabilities of the European XFEL Facility providing almost full transverse coherence (80%, with a beam of <1 mm^2 cross section) at 12.4 keV (Saldin *et al.*, 2006) and a high repetition rate of up to 5 MHz for FEL pulses. This time structure gives the possibility of studying dynamics in the submicrosecond regime and, using pump–probe arrangements, in the subpicosecond regime. This possibility opens up entirely new research horizons.

electronic reprint

In the last few years we have witnessed rapid development of CXDI techniques. Our experience is based at the moment on experiments that utilize the coherence properties of third-generation synchrotron sources. The coherent scattering volume at these sources is mainly determined by the source size and distance from the source and is typically about 10 μm in the horizontal direction and 100 μm in the vertical direction for 10 keV X-ray energy and at a distance of 50 m downstream from the source. The longitudinal coherence length is determined by the available monochromator and can reach $\sim$1 μm. The coherent flux is determined by the brilliance of the storage ring and is typically 10^{12} photons s^{-1} in the pink beam.

The possibility of single-pulse imaging with FELs was demonstrated recently in a proof-of-principle experiment (Chapman, Barty, Bogan *et al.*, 2006), when a test sample was imaged by phase retrieval with a single pulse containing 10^{12} photons at 32 nm wavelength using a FLASH facility in Hamburg. It was shown in this experiment that a coherent diffraction pattern can be recorded before the sample is destroyed by an intense FEL pulse.

CXDI is presently considered as one of the major areas of scientific research at the European XFEL Facility. With this in mind, we organize this paper in the following way. In the following section we give a summary of the scientific case, beginning with a short overview of the results obtained using CXDI at third-generation synchrotron sources, its limitations and possible applications using the XFEL source. The third section introduces requirements for CXDI experiments using FEL sources. Special attention is paid here to wavefront-preserving optics. The final section proposes a realisation of the CXDI instrument at the European XFEL Facility.

2. Scientific case

2.1. Present status: limitations at third-generation sources

At the moment, the development of coherent X-ray scattering can be distinctly divided into two main directions. One is based on Bragg scattering of the incoming coherent beam on small crystals; the other uses the forward-scattering geometry for non-crystalline objects. Both applications have their own advantages and limitations. In the case of Bragg diffraction, scattering angles are typically far away from the direct beam, so the whole diffraction pattern can be measured without the need of a beamstop, and there is no contribution from the beam-defining slits in the recorded diffraction pattern. On the other hand, scattering from non-periodic objects can be done only in the forward-scattering geometry, making the use of a beamstop in front of the detector unavoidable in many cases (for an exception, see Williams, Quiney *et al.*, 2006). As a result, there is a certain amount of missing information in the reciprocal space for small q-values in this scattering geometry. Using the Bragg approach it is easier to scan a sufficient region of reciprocal space with a two-dimensional detector to obtain fully three-dimensional information about the object. This can be done, for example, by performing fine angular scans near the Bragg peak or energy scans. In the case of scattering from non-crystalline objects, three-dimensional reconstruction is performed by measuring several diffraction patterns at different projection angles, as in tomography, and then reconstructing the object by iterative methods.

The following examples show that coherent X-ray diffraction of small crystals can provide us with information such as the crystal shape, internal structure and deformation field. Coherent X-ray diffraction imaging was for the first time applied to study the three-dimensional structure of micrometer-sized Au particles (Robinson *et al.*, 2001; Williams *et al.*, 2003; Williams, Pfeifer *et al.*, 2006). The three-dimensional real-space density corresponding to the reconstructed phase and measured amplitude of the CXDI pattern was obtained from those experiments. The internal density contrast was found to be in the form of bright and dark bands oriented parallel to both the [111] and [11$\bar{1}$] directions in the images. The [111] bands have a width of 50 nm, a period of 100 nm and a lateral extent of 600 nm, both within the section and between adjacent sections. The [11$\bar{1}$] bands have the same width and are slightly less extended. These features were interpreted to be deformation bands associated with sample preparation. The dark region of the band presumably corresponds to material with twinned stacking that would diffract in a direction different from the (11$\bar{1}$) imaging direction. Such bands are known to occur in soft face-centered-cubic metals and are attributed to recrystallization following slippage along [111] planes during deformation (Hayden *et al.*, 1965).

In the above example, special care was taken to grow unstrained crystals. However, it can be shown, under very general conditions (Vartanyants & Robinson, 2001), that if a coherent X-ray beam is scattered on a strained crystal, then the local symmetry around each Bragg peak is broken and the effect will be stronger at higher-order reflections. In the following example, equilibrium shapes of Pb nanocrystals were investigated (Pfeifer *et al.*, 2006). The shape of the crystals was reconstructed from the measured coherent diffraction patterns (Fig. 1) and, in addition, the projection of the strain field on the scattering vector **Q** was reconstructed (Fig. 2).

The resolution obtained in this experiment was estimated to be 40 nm, and the main limiting factors were the incoming flux (the measurement time was 150 s per frame) and the detector sensitivity. We believe that the XFEL can substantially improve the resolution by providing 10^{12} coherent photons in one pulse.

One of the most exciting applications of coherent XFEL beams in the future will be studies of quantum systems (quantum dots and quantum wires). This will be discussed in detail later in this chapter. Some initial experience and understanding of how coherent X-ray diffraction can be applied to quantum dot samples was obtained by Vartanyants *et al.* (2005) and Vartanyants & Robinson (2003). In the experiment (Vartanyants *et al.*, 2005), performed on a periodic array of Ge islands on Si, the diffracted intensities show all the main features predicted (Vartanyants & Robinson, 2003). However, they also contain a strong 'diffuse' scattered inten-

electronic reprint

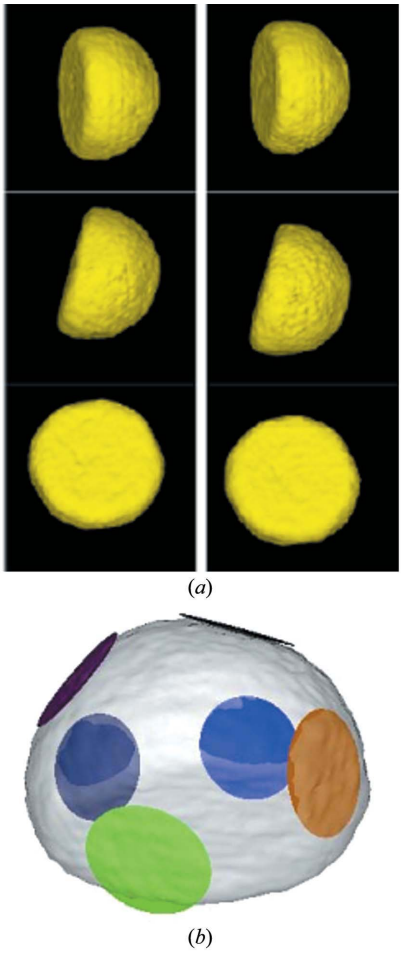

Figure 1
(*a*) Surface plots of Pb reconstructed shapes. Left and right columns corresponds to the two best reconstructions. (*b*) Three-dimensional view of (*a*) showing the fitted facet planes of the equilibrium crystal shape.

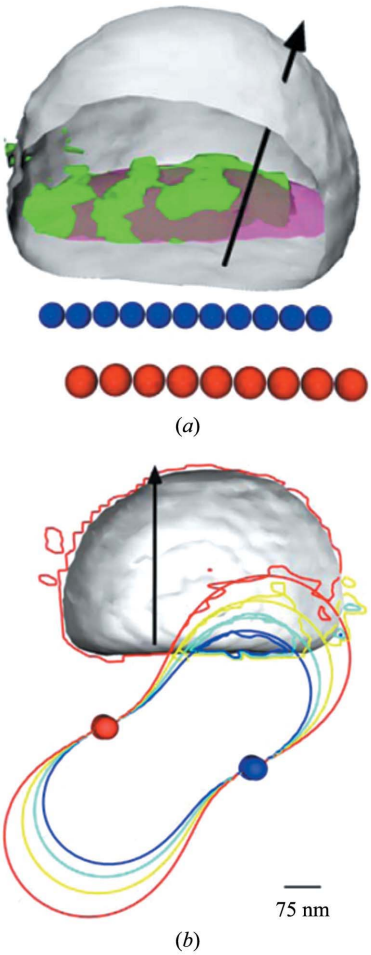

Figure 2
(*a*) Single isosurface of the phase and the best fit superimposed on a cut-away image of the crystal density. The point defect lines used to generate the fit (dots) and the direction of **Q** (arrow) are also illustrated. (*b*) Contour map of the cross section of the reconstructed phase of the complex density function on a plane passing through the middle of the nanocrystal. Smooth lines are the corresponding contours of the projection function $\mathbf{Q}\cdot\mathbf{u}(r)$, where $\mathbf{u}(r)$ is the strain field calculated for two rows of point defects (balls) of opposite sign. Both sets of contours have spacings of 0.24 rad.

sity that, in a coherent beam, consists of the complicated speckle pattern owing to inhomogeneities of individual quantum dots. Here, measurements on single quantum dots are expected to provide a much 'cleaner' diffraction pattern. We also think that imaging of two-dimensional periodic quantum dot structures could be an important step towards single molecule imaging.

It is clear that CXDI, especially with harder X-rays, is quite photon 'hungry': the coherent flux per spatially and temporally coherent mode scales as the inverse third power of the photon energy. Moreover, pushing coherent scattering techniques to study nanosized samples is even more demanding, as the number of elastically scattered photons decreases with the sample volume. The large coherent flux provided by the XFEL will be crucial for the success of these experiments.

CXDI experiments are also possible using predominantly forward scattering by non-crystalline objects. The single molecule imaging experiment is the most challenging example in this regard. Scattering in the forward direction is determined by the electron density distribution of the sample. First results showing a three-dimensional reconstruction of a structure by phase retrieval from its coherent diffraction patterns were reported by Miao *et al.* (2002). The three-dimensional reconstruction was carried out on a specially prepared test Ni sample using a series of 31 two-dimensional diffraction patterns recorded from the sample with rotation angles ranging from -75° to 75° in 5° increments. The resolution obtained in this experiment was estimated to reach 50 nm.

Recently, a three-dimensional reconstruction with a resolution of 10 nm × 10 nm × 40 nm using test samples and soft X-rays with energy 750 eV (1.65 nm wavelength) was reported (Chapman, Barty, Marchesini *et al.*, 2006), and a three-dimensional reconstruction of a 800 nm GaN particle with a voxel size of 17 nm^3 was demonstrated with hard X-rays by Miao *et al.* (2006). In the latter case, formation of small islands on the surface of the particle owing to nitrogen treatment were observed.

X-ray holography offers a complementary approach to iterative recovery of the object phase. Holography uses a well defined reference wave mutually coherent with the scattered

electronic reprint

object wave to encode the phase in the coherent diffraction pattern from the object. The complex amplitude of the object wave is recovered from the recorded hologram, down to the sign of the phase, by a single (non-iterative) numerical calculation. Various optical geometries for holographic imaging have been demonstrated with soft X-ray lasers (Trebes *et al.*, 1987; Bartels *et al.*, 2002), undulator sources (Eisebitt *et al.*, 2004; Howells *et al.*, 1987; Jacobsen *et al.*, 1990; McNulty *et al.*, 1992; Lindaas *et al.*, 1996) and hard X-ray undulators (Cloetens *et al.*, 1999). The reference wave can be planar or curved; under appropriate conditions a curved wave aids unique recovery of the phase (Nugent *et al.*, 2003; Xiao & Shen, 2005). As with CXDI, the recoverable object resolution is limited by the signal-to-noise ratio of the interference fringes recorded at the greatest momentum transfer Q in the coherent diffraction pattern. In holography experiments to date this has been restricted to the maximum Q of the reference wave that can be produced by X-ray optics such as pinholes or zone plate lenses. This currently corresponds to an object resolution of about 40 nm; this can be expected to improve to 15 nm (Chao *et al.*, 2005) and possibly to as high as 1 nm as X-ray optics continue to improve (Kang *et al.*, 2006; Schroer, 2006; Pfeiffer *et al.*, 2006). Fig. 3 is an example of a reconstructed X-ray hologram showing magnetic contrast using a coplanar pinhole to form the reference wave.

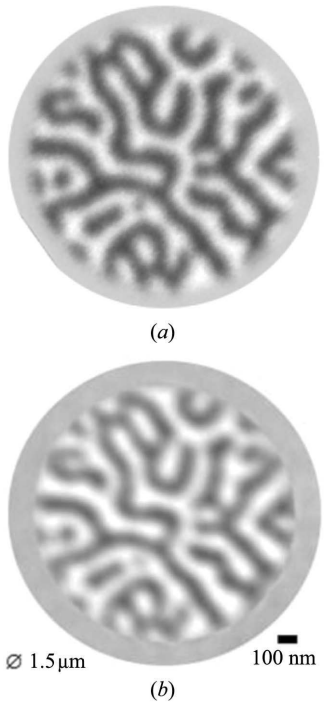

Figure 3
(*a*) Scanning transmission X-ray microscope image of a CoPt multilayer containing labyrinthine magnetic domains. (*b*) Reconstructed Fourier transform hologram of the sample, recorded at the BESSY UE56-SGM beamline. In both cases the difference between opposite helicities of circularly polarized light is shown to reveal the magnetic domains (Eisebitt *et al.*, 2004). [Reprinted by permission from Macmillan Publishers Ltd: *Nature (London)*, S. Eisebitt, J. Luning, W. F. Schlotter, M. Lorgen, O. Hellwig, W. Eberhardt & J. Stohr, *Nature (London)*, **432**, 885–888, (2004), copyright 2004.]

The experimental set-up and optics used for X-ray holography are readily shared with those used for CXDI in the forward-scattering direction. Consequently it is practical to record holographic interference fringes (*i.e.* with a mutually coherent reference wave) out to the momentum transfer permitted by the optics, simultaneously with the referenceless coherent diffraction at higher momentum transfer than the hologram fringes. This two-pronged approach is promising because the phase provided directly by the reference wave can be used to improve the speed and accuracy of iterative phase retrieval of the referenceless coherent diffraction at high momentum transfer (He *et al.*, 2004). The recoverable resolution in this scheme therefore is not limited by the X-ray optics used to form the reference wave and thus the hologram alone. A demonstration of this approach was recently reported using 1.8 nm soft X-rays and a focusing zone plate lens (Williams, Quiney *et al.*, 2006).

2.2. Applications of the XFEL

2.2.1. Nanomaterials. Today's high technology industry demands increasing miniaturization of device structures, mainly for integrated circuits in the semiconductor industry, but also of magnetic, optical and biological sensors. There has been a strong interest recently in the manufacturing and the characterization of structures on a nanometer scale, with the hope that the material properties of nanostructures can be tailored by changing their size, *via* quantum size effects. One important area is the development of next-generation magnetic storage media. Recent developments in this field are currently pushing the magnetic bit size below 100 nm. There has been considerable impact on our understanding of the growth and the structural properties of nanostructures through the use of scanning microscopy techniques, which enable us to achieve atomic resolution in real-space structural determination. However, similar experimental techniques to obtain element-specific electronic structure information on a nanometer scale are still lacking.

Despite the fact that many of the fascinating properties of nanoparticles can be exploited only for an ensemble of many particles, it may be of interest to study properties of a single particle. This would be of particular interest for *in situ* studies of catalytic or magnetic behavior. Alternatively, investigating ensembles requires non-interacting particles with exactly the same size in order to obtain information about a single particle.

In the following, a possible application of the European XFEL for structural investigations of nanocrystalline compounds in the form of single particles is presented. Rough estimates show that single bunch exposures of nanocrystalline materials with diameters of 100 nm to the focused beam will produce a diffraction pattern with enough statistics for phase retrieval. The proposed XFEL facility will therefore be of great interest for structural studies of two different classes of nanomaterials. The first class includes nanocrystals, *i.e.* materials with particle size in the range from 10 nm to 100 nm. Important groups of these materials are magnetic and

electronic reprint

dielectric thin films and crystals, metal alloys, and special ceramics based on oxides (Freund *et al.*, 1998). The second class of materials comprises the extremely fine particles of clays and clay minerals. These materials usually do show translation periodicity; however, they are in many cases highly disordered.

Owing to their small size, these materials cannot at present be investigated by single-crystal X-ray diffraction techniques. For the detailed structural analysis of single crystals, it is important to obtain integral Bragg intensities with high reliability. Therefore, it is necessary to establish a highly precise monitoring system for intensity, coherence and wavelength. An estimate of the sample sizes and exposure times that takes sample damage into account, based on a rough comparison with experiments at the ESRF, shows that, for a crystal of size 100 nm × 100 nm × 100 nm and the focused XFEL beam, diffracted intensities from a single bunch would provide a signal allowing the structure to be solved with sufficient accuracy. The information obtained from these data will be sufficient to determine the structure accurately (Bragg peaks) and the degree of disorder (continuous diffuse scattering). Ideally, if the whole crystal is coherently illuminated then the scattered intensity will produce a continuous diffraction pattern with high statistics that can be inverted and give the detailed structure of the defects in the crystal.

If sample degradation owing to radiation-induced damage turns out to be tolerable, much smaller samples will be feasible, offering the exciting prospect of studying individual single nanocrystalline particles using X-ray diffraction techniques. With increasing sample size and respective beam diameter, the time scale is reduced correspondingly. If, for example, 1 μm resolution is considered sufficient for the determination of the local structure fluctuation, a thin needle or flat sample of larger overall dimensions can be sampled with a primary beam size of 1 μm diameter. In this case an exposure of 600 ns is sufficient to record the diffuse scattering in a single orientation.

Particularly, for single-crystal diffraction of crystals with strongly fluctuating properties, the sample stability is of crucial importance. Whether samples will be stable under the intense XFEL beam cannot at present be answered with any degree of certainty.

One of the important targets in this area of research is quantum dot structures. Progress in nanoscience and nanotechnology requires tools to characterize the structure of objects both on the mesoscopic and atomic levels. This is especially relevant in semiconductor devices based on heterostructures, where one big challenge is the investigation of individual nanostructures, which is important to quantify differences in self-assembled structures and to correlate these differences with the particular nanostructure location on the sample. This will be increasingly important for nanostructures embedded in electronic devices.

Using coherent nanometer focused XFEL beams targeted on such samples could answer questions that cannot be solved with the present level of technology. Combining real-space mapping with nanometer resolution and coherent X-ray diffraction experiments could provide information about the size, shape, strain and chemical composition of individual nanostructures after a single pulse exposure.

Spatially resolved CXDI from low-dimensional systems will play an important role in understanding the structure, fabrication and functionality of many nanomaterials. The advancement of CXDI will have wide-ranging applications including the investigation of self-assembled and semiconductor nanostructures, surfaces and interfaces, extended defects, granular materials and many other systems.

The study of nanodomain imaging of ferroelectric thin films and crystals is another major area of basic research with a big potential impact on applications for electronic and photonic devices (Dawber *et al.*, 2005). Long-term operation of practical devices such as non-volatile FeRAM (ferroelectric random access memory) rely on consistent polarization switching over more than 10^{12} cycles of the applied field. For the investigation of domain configurations and orientations of domain walls on a nanoscopic scale in real life sample geometries a CXDI is especially well suited. The influence of inhomogeneous strain, defects and composition on polarization fatigue will be structurally accessible (Do *et al.*, 2004).

Magnetic nanodots are a field of extensive research and could find their applications in the future fast-switching memory devices. The possibility to image different magnetization in each nanodot of 100 nm size with a coherent Fourier holography approach was demonstrated recently (Eisebitt, 2007). Performing such experiments at XFEL will give an opportunity to image the magnetization switching at sub-ps time scale that cannot be done with present sources.

An important field of semiconductor nanoscience research nowadays is the investigation of single islands and a few coupled islands to obtain their electronic properties. For this purpose, microphotoluminescence (μ-PL) and photocurrent spectroscopy have been applied to measure transitions in neutral and charged single excitons (Finley *et al.*, 2004), mainly in InGaAs/GaAs quantum dot systems. For an interpretation of the results, model calculations based on the structure of the islands (size, shape, composition and strain profile, existence of facets) are performed (Finley *et al.*, 2004; Bester *et al.*, 2003; Narvaez *et al.*, 2005). Owing to fluctuations in the quantum dot ensemble, which are difficult to quantify, these models usually contain free parameters, rendering the simulations ambiguous to a certain extent (Narvaez *et al.*, 2005). Being able to determine the structural parameters of a single island, and correlate the results to μ-PL and photocurrent results at *the same island* would considerably further this field. Transmission electron microscopy (TEM) and cross-section scanning tunnel microscopy (STM) cannot be used for this purpose, as these methods are destructive and do not allow a specific quantum dot to be prepared for analysis. Using focused XFEL beams will make it feasible.

X-ray diffraction (XRD) has proven a powerful tool for the determination of composition and strain distribution in nanostructures. Several methods have been established, based on measuring the diffuse intensity distribution with high resolution in reciprocal space (Stangl *et al.*, 2003, 2004; Hesse

electronic reprint

et al., 2002; Wiebach *et al.*, 2000; Kegel *et al.*, 2001; Schülli *et al.*, 2003; Malachias *et al.*, 2003, 2005). While conventional local probe techniques such as TEM typically reach lattice parameter resolutions about $\Delta a/a = 10^{-2}$, XRD experiments easily reach values of $\Delta a/a = 10^{-3}$ to 10^{-4}. So far, large ensembles of typically 10^5 to 10^6 nanostructures have been investigated by XRD, providing statistically well averaged properties with a spatial resolution in the nm range for the *average object* under investigation. Focused XFEL beams, allowing high spatial resolution in addition to the high reciprocal space resolution, make the analysis for a *specific nanostructure* on the sample feasible. Considering the typical dimensions, an area with an extension of not more than about 100 nm has to be illuminated.

There has been considerable progress in recent years with X-ray focusing devices, and several groups have demonstrated focus sizes around or even below 100 nm (Chao *et al.*, 2005; Kang *et al.*, 2006; Schroer, 2006; Pfeiffer *et al.*, 2002, 2006; Quiney *et al.*, 2006; Schroer *et al.*, 2003; Schroer & Lengeler, 2005; Jarre *et al.*, 2004, 2005; David *et al.*, 2001; Di Fonzo *et al.*, 2000). Using XFEL beams will be beneficial because, owing to a high degree of coherence, diffraction-limited focusing can be achieved, providing the smallest possible focus size and preserving full coherence across the beam.

One of the possible projects on XFEL can be the further development of the coherent X-ray diffraction imaging technique, with its application to single islands of semiconductors coherently grown on a substrate (like SiGe dots on Si). One of the most important outcomes of the whole project will be model-free determination of the anisotropic strain distribution in a single island (including buried ones) and in the substrate.

2.2.2. Three-dimensional structural characterization of mesoscale systems. Investigating the mesoscale or nanoscale properties of hard materials has become a focus of the hard condensed matter community. In contrast to the atomic and macroscopic scale, our understanding of the structure on this scale is less mature. In particular, models tend to be based on average properties, despite the fact that the materials often are very heterogeneous on this scale. As an example, the macroscopic properties of metals such as strength or fatigue are governed by the properties of grains and dislocation structures and their interactions. The properties of the objects vary by orders of magnitude depending on factors such as size and crystallographic orientation. Present structural techniques cannot characterize this heterogeneity.

Neutron diffraction lacks the spatial resolution for observing the 'building blocks'. Electron microscopy, on the other hand, probes only the surface. As such it can be used only for '*post mortem*' study of sectioned samples. The dynamics cannot be probed, and interactions between objects cannot be observed directly. Also, heterogeneous structures tend to be truly three-dimensional, and sections can be misleading. Only recently, with third-generation X-ray sources, it has become possible to obtain static information from each individual grain of micrometer size (Larson *et al.*, 2002). We believe that by using CXDI and with the power of XFEL we can investigate structural properties of mesoscale systems in three dimensions with nanometer resolution. Some applications to magnetic and dielectic materials, metal and ceramic systems are described in the following paragraphs.

Magnetic and dielectric materials. Use of circularly polarized X-rays from the XFEL and tuning the energy to the *L* and *M* edges of appropriate elements would enable sensitivity to electronic spin and charge orientation in magnetic materials, crystals and thin films by means of resonant X-ray dichroism contrast. By taking advantage of the ultrafast XFEL pulses one could probe fundamental time scales for magnetic phase transitions, spin-coupling, and precessional switching and reversal spin-torque devices. The ability to probe nanometer spatial scales would be valuable in order to clarify, for instance, the inner bit structure of nanopatterned magnetic media. The ultimate challenge would be to image electronic spin switching on the femtosecond scale. The XFEL would similarly be useful for time-resolved study of domains in dielectric materials and multiferroics exhibiting piezomagnetism and piezoelectricity, for example, to investigate electric-field-driven phase transitions and dielectric breakdown in insulators such as lead zirconium titanate and bismuth ferrite.

Metals. Typical metal structures are presented in Fig. 4, displaying the four inherent length scales (Poulsen, 2004). Grain structures in well annealed metals have typical sizes of 1–100 μm and are very homogeneous, as can be seen in Fig. 4(*a*). Application of stress leads to deformation and the

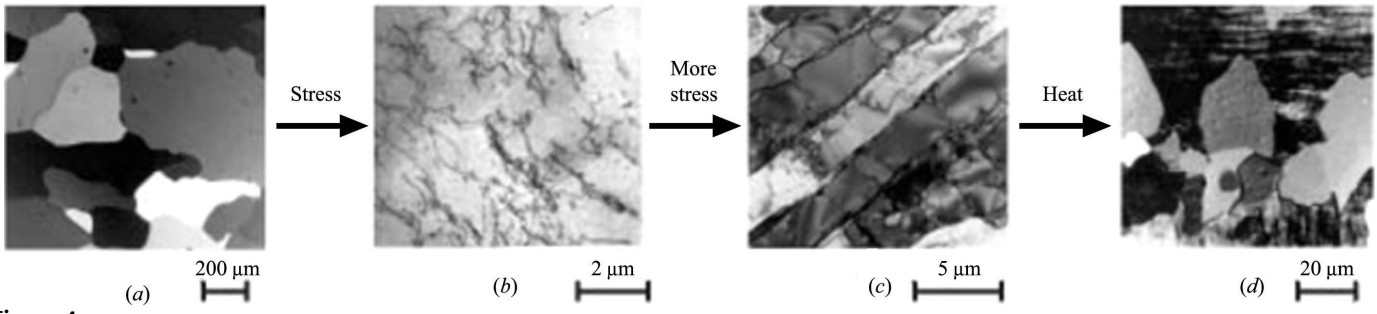

Figure 4
Metal structures as observed by non-X-ray microscopy. The micrographs correspond to snapshots in time for random locations after exposure to stress and heat. No direct information about dynamics can thus be obtained using this method. (*a*) Initial grain structure of a metal. (*b*) A well annealed grain structure shows evidence of tangled dislocations after some deformation. (*c*) With more deformation, these form into dislocation structures. (*d*) Upon annealing, new nuclei form and grow from this deformed matrix.

electronic reprint

formation of individual dislocations at length scales 0.1–1 μm (Fig. 4*b*). Increasing the deformation leads to dislocation structures on the few micrometer scale (Fig. 4*c*). Upon annealing, new nuclei are formed which grow from the matrix and show no dislocations (Fig. 4*d*). The processes of deformation and annealing are important in the 'life' of every material, and it is evident that dynamic, *e.g.* time-resolved, data will help in understanding the underlying processes. Such data can only relate to the bulk of the material, as the surface is non-representative owing to stress relaxation, dislocation migration, pinning on surface grooves *etc.* The following specific questions of vital interest motivate such three-dimensional structural investigations to include:

(i) How do dislocation structures emerge from individual dislocations?

(ii) How do grains and dislocation structures deform?

(iii) Nucleation: where in the deformed material do nuclei form, and what are the orientation relationships between nuclei and the sites at which they form? What is the nucleation mechanism?

(iv) Growth: how do the nuclei grow, what are the kinetics as a function of the relative orientations of the nuclei and the surrounding dislocation structures? Does the morphology of the dislocation structure play a role? How are the various types of dislocation structures actually absorbed into the moving interface of the nuclei?

These topics have been addressed in much detail by traditional means, but answers have been elusive. The XFEL combined with CXDI should be able to provide answers to some of these questions. Furthermore, combined dynamic investigations will be possible on three of the inherent length-scales: those of the sample, grain and dislocation structure. Hence, such data will be instrumental in the development of global models that bridge the length scales; in other words, in anchoring the macroscopic properties of interest to engineers to the mesoscale properties. The case for (industrial) alloys is similar, with the addition that the simultaneous use of tomography will be helpful in mapping and identifying secondary phases, inclusions *etc.*

Ceramics. Modern ceramics tend to be heterogeneous partly because non-equilibrium parts of phase diagrams are used and partly because function/cost considerations dictate the use of several components (multilayers, inclusions). The kinetics of the reactions, phase transformations *etc.* depend on the local environment of the grains, whether in the form of powders or sintered pellets. Again, surface studies are non-representative as the diffusion mechanisms are different. By providing local-scale information, ceramics processing will take a major step away from the present state of trial and error.

The study of grain dynamics using the XFEL source combined with CXDI will allow the kinetics of the individual grains to be observed without locating the exact positions of the grains. This will be a substitute for conventional *in situ* powder diffraction. 'Single crystal' structure refinements are applied here. In this way a statistical study can be performed based on groups of grains with specific volume, orientation and/or stoichiometric properties. Furthermore, reactions between neighboring grains can be observed directly by high-resolution mapping. The resolution of a few nanometers fits well with the grain size of many powders. The combination of diffraction and imaging is especially attractive in this case, since structure and density of the various grains are often unknown.

2.2.3. Dynamic processes and time-resolved investigations of fluctuations. One potential of the XFEL lies in the ability to measure the time evolution of transient structures on the 200 ns time-scale of the XFEL pulse spacing. The 100 fs exposure time of a single bunch might catch a spontaneous fluctuation on that time scale. It is estimated that crystalline objects 10 nm across would give measurable diffraction patterns, and objects 100 nm across would be measurable during a single XFEL pulse. This type of application requires all the special properties of the XFEL: a coherent beam for the imaging, intensity because of the minute object size, and short time structure for time-resolved experiments. In this regard, CXDI experiments could also take advantage of pump–probe methods being developed for other XFEL experiments such as XPCS.

Another possible application of coherent femtosecond X-ray pulses will be for study of the surface dynamics. Consider a crystal surface with an area of only a few square micrometers. The coherent XFEL produces enough photons to fully characterize such an area in one bunch train, thus in <1 ms. It will thus be possible to see step dynamics on the time scale of successive bunch trains ($\sim$100 ms). The dynamics can be caused either by statistical fluctuations or by growth or etching. This imaging would not only be faster than is currently possible, but could also be applied to systems under high gas pressure or at high temperature, or to surfaces buried under a solid or liquid, for which there are no alternative techniques. On a much slower time and larger length scale, a silicon wafer has been imaged in this way during the etching of the native oxide (Robinson *et al.*, 1999).

Of considerable scientific interest are the spontaneously nucleated clusters of a crystalline solid in an aqueous solution close to saturation. Time-resolved experiments with the XFEL would permit testing of the microscopic theory of classical nucleation, which has not been possible before. According to theory, solute molecules randomly associate into clusters with a thermodynamic equilibrium distribution, so that the largest clusters are the scarcest (Fig. 5). Once a cluster exceeds the critical nucleus size, it becomes thermodynamically stable and grows into a macroscopic crystal. In standard nucleation theory, a smooth size distribution of small crystallites is assumed to be present up to the critical nucleus size. However, one can imagine that in reality the size distribution is not smooth, but that certain sizes are preferred. In the case of two-dimensional nucleation on metal surfaces, such magic clusters have been observed using STM (Rosenfeld *et al.*, 1992). The sub-critical nuclei may also have a shape or structure that deviates substantially from that of the bulk crystals that eventually grow out of them. Since we are interested in atomic scale fluctuations upon a large background of parent material,

electronic reprint

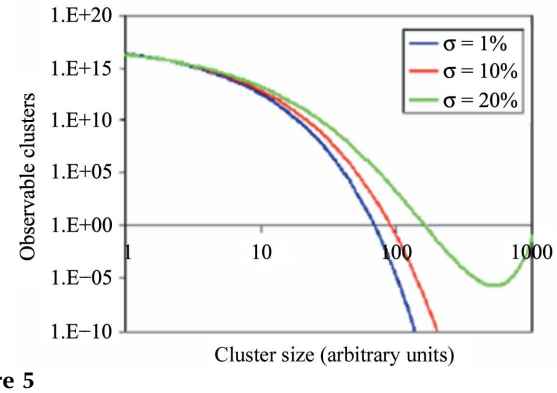

Figure 5
An estimated cluster-size distribution as a function of supersaturation σ according to standard nucleation theory. Only a few clusters exist at an appreciable size.

it is advantageous to concentrate the beam onto a reasonably small sample volume of the order of 1 μm^3 in order to improve statistics.

Possible systems for study fall into the general category of crystalline fluctuations in disordered matter, induced by some excitation such as temperature. For metals research, suitable examples are the local ordering of a binary alloy above its critical temperature or composition fluctuations in amorphous metal alloys. Alexander & McTague (1978) proposed there would be body-centered-cubic phase fluctuations in liquid face-centered-cubic metals. These have been confirmed in simulations by Shen & Oxtoby (1996) and by Klein (2001).

Fluctuations in aqueous solution are also of interest. Concentrated salt solutions, close to saturation, are expected to have critical fluctuations of the crystalline phase. When these 'pre-critical' nuclei become sufficiently large, they nucleate into actual crystals. The expected time scale of the fluctuations will depend enormously on the degree of supersaturation, which can be controlled by temperature, for instance. The 100 fs pulse of the European XFEL will easily be short enough to obtain snapshots of them. There is also a large field of study of binary mixtures of fluids that show phase separation into ordered structures that could be detected by diffraction. Self-assembling molecular and biological systems might be accessible also if there is a characteristic length scale established that would lead to diffraction.

In some cases the fluctuations will be rare events with a characteristic signature of a particular Bragg angle where the parent crystal structure diffracts. Here the experiment would be run at the highest framing rate that the detector bank can achieve, with a corresponding rate of single XFEL pulses, synchronized to the readout. The data stream would be monitored for 'trigger' events such as the appearance of speckles more intense than some threshold. This is analogous to the measurement strategy used in high-energy physics. Only the data immediately before and after such triggers would need to be saved for subsequent analysis. These measurements could also be performed with high-energy spontaneous radiation for sampling of a larger volume.

Other cases would produce a continuous stream of speckle snapshots, uncorrelated between frames because the fluctuations would be too fast. Statistical analysis of the distribution of speckles on each frame would be used to obtain the higher-order correlation functions of the nascent ordering under investigation. Presently, theoretical work (Mecke, 2007) has started to extract the interesting higher-order correlations, *e.g.* three-point correlation functions. Theoretical considerations combined with conventional coherent diffraction data, obtained from amorphous alloys for example, could be used to anticipate the kinds of correlations that might be interesting in a given system. Very good statistical evaluation of these higher-order correlation functions could be obtained by automated processing of the data stream. The experiment would then consist of varying the sample temperature or composition systematically. Special detector readout schemes or streak camera methods might be introduced to observe the lifetime of these fluctuations.

To illustrate the kind of data that might be obtained with a snapshot experiment during a pre-crystallization fluctuation, we calculated the diffraction pattern of a 10^3 atom cluster from a molecular dynamics simulation of freezing, shown in Fig. 6. The amplitude of its Fourier transform, shown in Fig. 7, represents the square root of the intensity that would be measured with a single European XFEL pulse. Because this is oversampled, it should be directly phaseable, and hence invertible to (projection) images of the fluctuation. The size of the simulation represents a volume of less than 10 nm^3, which is slightly less than can be achieved with focusing. A similar fluctuation within a larger volume will give the same signal, but more structured background.

Nanoscale phase separation is a phenomenon which is widespread in strongly correlated oxides, *e.g.* manganites and cuprates (Dagotto, 2005*a*). It causes interesting effects, such as colossal magnetoresistance in manganites, and it also appears crucial to understanding high-temperature superconductors. There is a spontaneous emergence of electronic nanometer-scale structures in transition metal oxides accompanied by the existence of many competing states involving charge, spin, orbital and lattice degree of freedoms. In manganites the competing phases involve ferromagnetic metallic, ferromagnetic insulating, and antiferromagnetic insulating phases whereby the insulating behavior is accompanied by charge or/and orbital order. Particularly in the presence of quenched disorder (chemical doping), inhomogeneous phases evolve. In cuprates there is evidence that an antiferromagnetic phase with charge ordered stripes is competing with a superconducting phase. Whether this state is a phase fluctuating homogeneous one or locally inhomogeneous is of ongoing discussion. Certainly, in the superconducting state of the cuprates and the metallic state of the manganites the inhomogeneities are not frozen; instead they are dynamically fluctuating.

The behavior of the antiferromagnetic domains which carry no external magnetic dipole moment but have a periodic arrangement of the electron spins extending over the macroscopic distances are still under debate. Recent X-ray correlation spectroscopy measurements on elemental chromium (Shpyrko *et al.*, 2007) have shown dynamics of these domains

electronic reprint

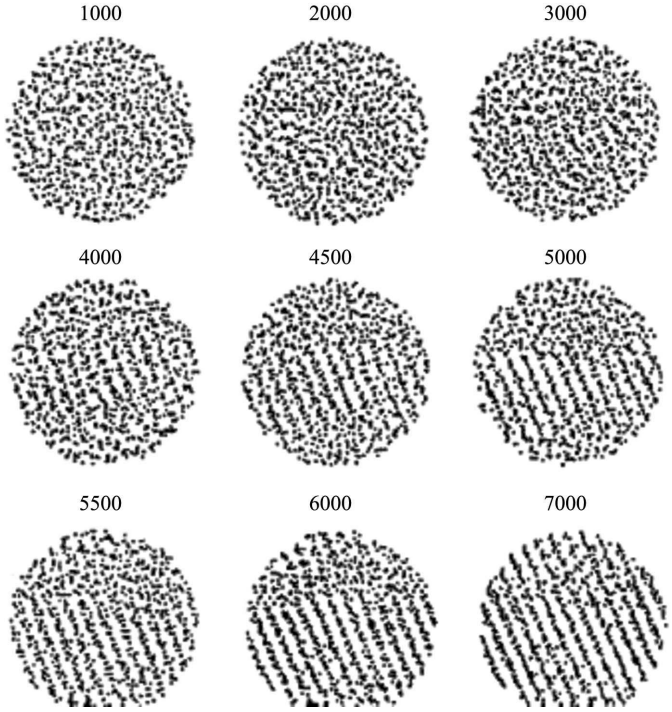

Figure 6
Molecular dynamics simulation of the freezing of a Lennard Jones liquid of 864 atoms as a function of time steps after a temperature jump (Nosé & Yonezawa, 1986). [Reused with permission from Shuichi Nosé and Fumiko Yonezawa, *Journal of Chemical Physics*, **84**, 1803 (1986). Copyright 1986, American Institute of Physics.]

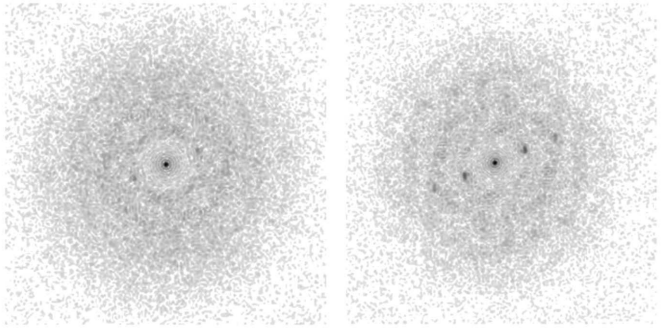

Figure 7
Simulated diffraction patterns of the atomic distributions simulated in Fig. 6, for the 1000th (left) and 5000th (right) time step.

on the 100 s time scale. Using coherent imaging techniques at XFEL should provide the means to see the frozen structure of these antiferromagnetic domains with their evolution in time.

CXDI could take advantage of the time structure of the XFEL and catch the scattering signatures of the fluctuating inhomogeneities on a 100 fs time scale with the added possibility of performing pump–probe studies. These scattering signatures could be resonant or non-resonant scattering in the hard or soft X-ray regime owing to charge and orbital order and their concomitant lattice distortions. Proper phase retrieval should give a detailed real-space picture of the inhomogeneous state of these complex systems and will allow many of the open questions, not only in manganite and cuprate physics, to be answered (Dagotto, 2005*b*).

2.2.4. Dynamic processes in metals and ceramics. The understanding of reactions during materials processing will have a new basis when experimental data and correspondingly refined modeling at spatial resolution below 1 μm and temporal resolution below 1 μs become available. Real-time small-angle X-ray scattering analysis may further be performed to analyze dissolution or coarsening of precipitates or pores with sizes smaller than ∼1 μm, whereas the opening and closing of larger pores, formed for example during creep, or close to a crack tip, may be measured using radiography under varying external load. Thus, comprehensive three-dimensional pictures of local microstructures may be derived with information content close to that obtained by the use of electron microscopy. A few examples from prominent areas have been selected below and indicate that time-resolved hard X-ray measurements at the XFEL can improve to a great extent the present-day knowledge of processing technologies. This applies equally well to techniques not mentioned yet, like extrusion, powder processing, sintering, cutting, carburizing, rapid solidification and joining. Even extremely fast processes like brittle cracking or fast deformations of materials by shock waves can be analyzed.

Real-time investigation of welding. The high intensity and repetition rate of XFEL pulses will allow novel real-time analysis of fast materials processing. For example, the *in situ* study of fast formation and deformation of grains, as well as precipitation reactions during welding, will become feasible. This will greatly increase our basic understanding of formation of microstructures in welds, which is regarded as an excellent basis for improving this joining technology. Time-resolved hard X-ray measurements at the XFEL laboratory are expected to greatly improve our knowledge of further processing technologies.

Precipitates and pores. The anticipated time resolution will allow the analysis of extremely fast growth and shrinkage of precipitates or pores. These effects may occur, for example, near crack tips, during melting, during solidification and fast cooling of droplets in powder processing, or during laser treatments of surfaces with local melting and fast cooling afterwards. Further novel analysis will be based on the extreme intensity of beams with areas even less than 1 μm^2 which may allow tomographic small-angle X-ray scattering investigations to be performed. These may be performed simultaneously with grain mapping so that spatial variations of sizes and number densities of precipitates and pores may be derived. Such analysis will, for example, significantly improve our basic understanding of failure mechanisms of materials around crack tips or the incoherent formation of creep pores in alloys and ceramics (Riedel, 1992).

Ultra-short-pulse laser interactions with matter. The interactions of high-power short-pulse lasers with materials have recently aroused a lot of interest in both the scientific community (Stuart *et al.*, 1995, 1996*a*) and the technological arena (Stuart *et al.*, 1996*b*; Neev *et al.*, 1996; Feil *et al.*, 1998; Perry *et al.*, 1999). On the one hand, understanding of the fundamental processes and basic mechanisms such as energy transfer from laser field to material, energy transport and

electronic reprint

subsequent athermal or thermal modifications in the material are largely lacking. On the other hand, technological processes such as laser drilling (*e.g.* Exarhos *et al.*, 1999) and cutting, machining (Perry *et al.*, 1999) and peening, and laser ablation for thin-film deposition (Stuart *et al.*, 1996*a*) have now been developed as alternative and replacing technologies for conventional processes. Laser damage in optical materials (Exarhos *et al.*, 1999) presents technological roadblocks to hi-tech processing of materials.

Given the femtosecond time structure and extremely high brilliance of XFEL sources, the dynamics of ultra-short-pulse laser interactions with matter may now be explored experimentally by using a variety of time-resolved and spatially resolved techniques. These include diffraction, imaging and a whole host of spectroscopic methods to capture and record modifications in crystal structure, phase transformation (Siders *et al.*, 1999; Rouhi *et al.*, 1999), morphology and microstructure evolution, which occur during the time the material 'sees' the laser light. Such dynamical data will in turn help to verify existing models and to construct new and better models of laser–matter interaction processes. These advances will further our basic understanding of laser-based technologies and help us to improve and develop them for future material processing and fabrication.

One of the possible applications can be the study of short-pulse laser ablation which is a promising process for nanoscience applications owing to the low threshold for material removal from surfaces. In the laser-ablation process, solid material transforms into an unsteady phase initiated by a rapid deposition of energy. Different pathways for non-thermal excitation can be present for very short laser pulses (Stuart *et al.*, 1996*b*). In a recent paper (Plech *et al.*, 2006), an ablation of gold particles of nanometer size induced by optical femtosecond excitation from a laser was studied. However, the time resolution for this study was limited by the pulse structure of the third-generation synchrotron source (the ESRF in this case). One could extend these studies to the XFEL facility when the ablation process can be studied at femtosecond resolution. In addition, if analysis of the paper (Plech *et al.*, 2006) was based on the modeling of small-angle scattering data collected from a large amount of particles, we could foresee similar experiments using XFEL pulses focused on a single particle that will give enough diffracted intensity to reconstruct the shape of the nanoparticle before and after interaction with optical pulse.

3. Requirements of the instrument

The experiments described above lead to requirements for an instrument for scientific applications using CXDI techniques. They concern the performance of the light source, optical elements, diagnostic equipment, sample environment and detectors.

Table 1
Relative merits and requirements of coherent full-field transmission X-ray imaging, X-ray holography and CXDI.

	Full-field	Holography	CXDI
Resolution limit	Optics	Reference	Detector
Feasible resolution	$\sim$10 nm	$\sim$10 nm	$\sim$1 nm
Optics required	Yes	Yes	No
Coherence required	No	Yes	Yes
Focusing required	Yes	No	No
Reference required	No	Yes	No
Direct method	Yes	No (one step)	No (iterative)
Phase retrieval needed	No (in focus)	Yes (one step)	Yes
Twin image problem	No (in focus)	No (unless in-line)	No
Signal dynamic range	Low	High	High
Compatible with CXDI	No	Yes	

3.1. X-ray optics requirements

The relative merits of X-ray microscopy methods suited to XFEL sources are compared in Table 1; coherent full-field transmission X-ray imaging, X-ray holography and CXDI are described. Holography provides the full complex amplitude of the object in one reconstruction step, whereas lensless CXDI is promising for obtaining the highest spatial resolution.

In previous reports the term 'coherence preserving optics' had been used to describe the quality of optical elements when used with the almost fully coherent radiation of the XFEL. This term is somewhat misleading, because an optical element, no matter how strong its aberrations and distortions, cannot degrade the coherence of the radiation, meaning that it will not reduce the fringe visibility of any diffraction or interference experiment. However, experiments aiming to retrieve amplitude and phase right after an object require a well defined phase of the incoming wavefront. While this phase is well known for a coherently illuminated aberration-free perfect optic, an imperfect optic will introduce wavefront distortions which are usually unknown and thus difficult to correct for. Therefore, the terms 'wavefront preserving' or 'diffraction limited' seem to be more appropriate for describing optical elements, in particular with respect to the precision required for nanometer-scale CXDI. Results with diffraction-limited focusing by diffractive lenses on the 15 nm scale are promising in this case (Chao *et al.*, 2005). In fact, the condition for yielding a well defined 'clean' wavefront may turn out to be more relevant for optics than the ability to achieve the smallest spot sizes. A situation where the wavefront illuminating the sample is unknown or, even worse, changes in time, must be avoided for the CXDI experiments.

The requested beam size in most experiments will be of the order of 0.1–1 μm. This is needed to limit the sample volume so that not too many fluctuations are sensed, and to concentrate the flux on the region of interest. The average heat load on the sample is not expected to be a serious problem because this is the same as at existing sources, but there will be considerable power levels over the duration of the pulse which could cause plasma formation. However, it seems unlikely that a crystalline nucleus would be completely disrupted on the time scale of the XFEL pulse duration. Further discussion on

electronic reprint

this topic and theoretical input on the 'meaning' of temperature will certainly be needed.

3.1.1. Beamline optics and metrology. Monochromator and mirror surfaces in an XFEL beamline are most subject to the tremendous heat load as they are closest to the source and they are hit by the full spectrum of the radiation. On the other hand, the radiation is spread out over a fairly large footprint of a bulk solid substrate facilitating heat dissipation. In this respect the best possible choice for monochromator crystals would be diamond, and recent progress in the fabrication of large synthetic diamond crystals suggests that this should be a feasible solution. Nevertheless, the shape error and slope error budgets of the reflecting elements surfaces required to control the wavefront over a size of several millimeters are beyond what can be bought today. In fact, the metrology tools available are one of the most severe limitations in the mirror fabrication process. Moreover, even a perfect mirror or monochromator surface may be distorted in the beam either by thermal load or by the mounting itself. This is why it is necessary to develop techniques to measure the distortions of X-ray wavefronts *in situ*. A precise knowledge of the wavefronts could then be the basis to learn about the properties of the source itself, to test and improve the optical components, and may even serve to compensate for errors of the illuminating X-ray wave.

An approach to performing *in situ* metrology has been developed recently at the Paul Scherrer Institute, Switzerland. The method is based on a hard X-ray interferometer as shown in Fig. 8. It consists of a phase grating as a beam splitter and an absorption grating as a transmission mask for the detector. The device can be used to measure wavefront shape gradients corresponding to radii of curvature as large as several dozens of meters, with a lateral resolution of a few micrometers. This corresponds to detected wavefront distortions of approximately 10^{-12} m or $\lambda/100$. The device was used with 12.4 keV X-rays to measure the slope error and height profile of multilayer mirrors (Weitkamp *et al.*, 2005) and beryllium refractive lenses (Weitkamp *et al.*, 2007). A similar set-up could be used at the XFEL to investigate the quality of beamline optics under the extreme conditions of this machine.

3.1.2. Focusing optics. For a number of experiments at the XFEL, focusing the X-ray beam to a small spot is desirable to increase the photon density at the sample position. This means that the lenses apertures should be as large as the beam to collect as many photons as possible. If the optics are illuminated with a fully coherent beam, the focused spot size will

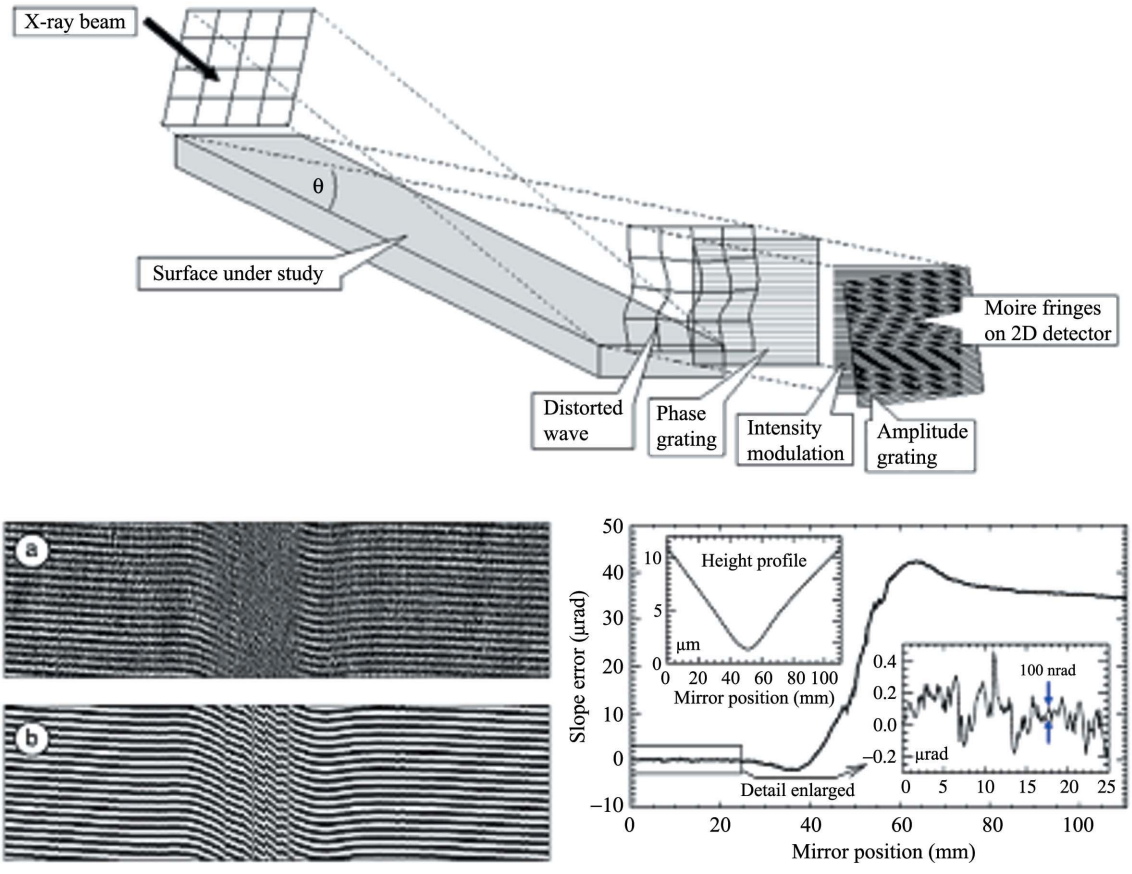

Figure 8
Set-up for the measurement of hard X-ray wavefront distortions using a shearing interferometer consisting of two gratings and a two-dimensional detector (top). The method can be used to measure the properties of an XFEL wavefront or its optical components such as monochromators and mirrors *in situ*. By analyzing the distortions of the recorded Moiré patterns (bottom, left), the slope error of the reflecting surface or the wavefront can be derived with an accuracy of better than 0.1 μrad (Weitkamp *et al.*, 2005).

electronic reprint

Table 2
Current performances of hard X-ray extreme focusing optics.

	KB mirrors	Nanofocusing refractive lenses	Fresnel zone plates
Achieved focal spot (nm)	36 × 48 (15 keV, mirror; Mimura *et al.*, 2006); 45 (24 keV, ML; Hignette *et al.*, 2006)	47 × 55 (21 keV; Schroer *et al.*, 2005)	∼150 (12.7 keV; Nöhammer *et al.*, 2005)
Aperture (μm)	100 × 100	30 × 40	50–300 (circular)
Efficiency	Close to 100%	20%	Typically 10%
Thermal stability	Good	Excellent	Poor (transmission), good (reflection)
Diffraction limited	No	No	Yes
Scalability to 1 mm aperture	Difficult	Not applicable	Possible

no longer depend on the source size or the demagnification factor. It will be diffraction limited in the case of a perfect optic and aberration limited in the case of a non-perfect, *i.e.* distorted, optic. As mentioned before, experiments that aim to retrieve amplitude and phase right after an object require a well defined phase of the incoming wavefront. While this phase is well known for a coherently illuminated aberration-free perfect optic, an imperfect optic will introduce wavefront distortions which are usually unknown and thus difficult to correct for. It is therefore important to learn whether or not focusing optics can preserve the wavefront quality to the precision required for nanometer-scale CXDI. In fact, the condition to yield a well defined 'clean' wavefront may turn out to be more relevant for such optics than the actual size of the spot itself.

Focusing X-ray optics can be divided into three classes that all have their advantages and drawbacks depending on the specific application, photon energy, achievable spot size and aperture, and robustness: (i) reflective, (ii) refractive and (iii) diffractive. [Waveguides have also been used successfully to produce very small hard X-ray spot sizes (Jarre *et al.*, 2005), but owing to their small working distance and relative inefficiency compared with other focusing optics they are not likely to find broad use at XFEL sources.] A brief review of the present state-of-the-art for hard X-ray nanofocusing and the future potential with respect to the specific requirements in context with the XFEL will be given, and is summarized in Table 2.

Mirrors. High-resolution X-ray mirrors are usually built in Kirkpatrick–Baez (KB) geometry. Significant progress has been made in the past year. The best spot sizes are of the order of 50 nm for single-surface mirrors (Mimura *et al.*, 2006) and multilayer mirrors (Hignette *et al.*, 2006). Typical apertures are 100 μm, which is matched to the transverse coherence lengths of third-generation insertion-device beamlines. The performance is still limited by the figure errors of the mirror surfaces. So far, diffraction-limited resolution has not been achieved, but the metrology and surface machining is continuously improving so that this may be possible in the near future. Damage by the high thermal loads of the XFEL seems unlikely, as the power is distributed over a large footprint of a bulk substrate, but even slight thermal deformations would deteriorate the focusing capabilities. A scaling up of the present apertures to collect the whole coherent flux from the source will be very difficult, especially when high (or even diffraction limited) resolution is required, as the length of the mirror substrates has to increase. In this respect, multilayer (ML) mirrors are probably the more promising approach as they require much shorter lengths owing to the higher reflection angles.

Refractive lenses. The classical compound refractive lenses consisting of stacked Al or Be discs with embossed parabolic depressions on the optical axis are very robust devices commonly used at synchrotron beamlines. Their geometry and materials make them well suited to withstand the enormous heat loads of an XFEL. At current synchrotron radiation sources, focusing is source-size limited, and a diffraction-limited focus is not reached with these optics. For Be lenses with about 1 mm aperture, however, the diffraction limit could be as low as 50 nm. This has, however, not been demonstrated so far. Resolution values similar to those achieved using KB systems (∼50 nm) can be obtained today using so-called nanofocusing lenses (NFLs). Similar to KB systems, two devices have to be used with orthogonal orientation to obtain two-dimensional focusing. The geometry is ideal for heat dissipation into the solid substrate, and the resistance to extreme peak power would require these optics to be made of a low-Z material, such as diamond (see Fig. 9). This would reduce absorption and improve heat conductivity. The presently obtained apertures are limited to a few tens of micrometers by the fact that the structures have to be etched into the substrates with sufficient smoothness and orthogonality of the sidewalls. The silicon NFLs shown in Fig. 9 have almost reached diffraction-limited performance. NFLs have the potential of generating diffraction-limited foci down to the sub-20 nm range. However, their aperture is intrinsically small.

Diffractive optics. At present, the best resolution for X-ray focusing is obtained by using diffractive optics such as Fresnel or multilayer-Laue zone plates (ZPs). ZPs have demonstrated a resolution beyond 30 nm (Chao *et al.*, 2005; Kang *et al.*, 2006). The ultimate resolution of a ZP is of the order of the smallest outermost zone width, meaning that nanolithography processes with sufficient resolution have to be applied. State-of-the-art electron-beam lithography and multilayer deposition tools are capable of placing the diffracting structures with lateral placement accuracies of a few nanometers, *i.e.* within a fraction of the outermost zone width. As a consequence, the wavefront precision is controlled to within a fraction of a wavelength, and diffraction-limited resolution is routinely

electronic reprint

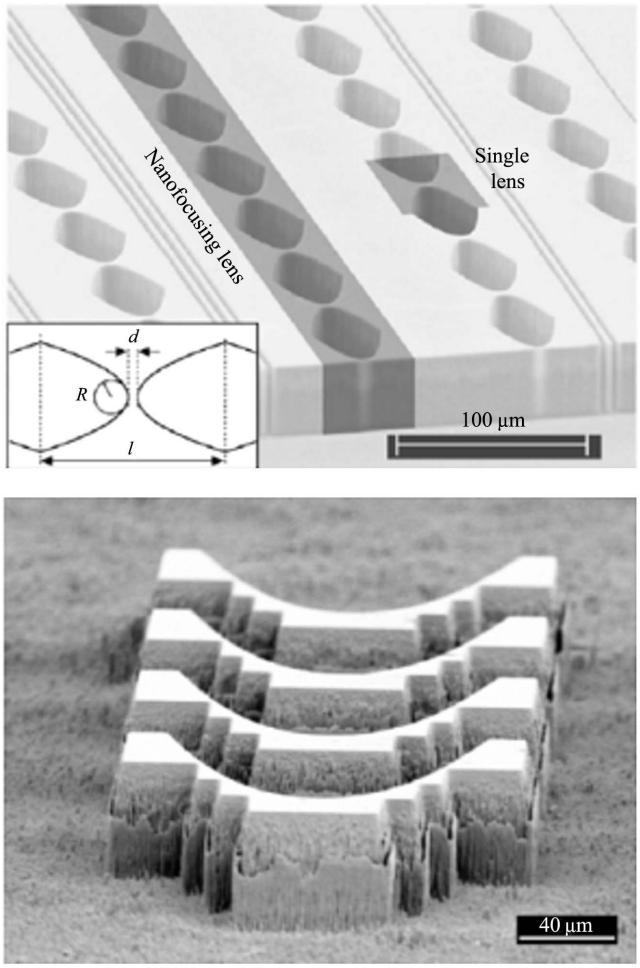

Figure 9
Top: nanofocusing lenses made by electron-beam lithography and reactive ion etching of silicon (Schroer *et al.*, 2005). [Reused with permission from C. G. Schroer, O. Kurapova, J. Patommel, P. Boye, J. Feldkamp, B. Lengeler, M. Burghammer, C. Riekel, L. Vincze, A. van der Hart and M. Küchler, *Applied Physics Letters*, **87**, 124103 (2005). Copyright 2005, American Institute of Physics.] Bottom: diamond planar refractive lenses fabricated using a similar technique (Nöhammer *et al.*, 2003).

achieved when sufficient transverse and longitudinal coherence is provided. Efficient focusing of hard X-rays by ZPs is more difficult because the zone structures must be sufficiently dense and thick to provide a phase shift near π for best diffraction efficiency. The zone structures are typically made from heavy metals, and they must be of the order of 1 μm thick for hard X-ray focusing. Owing to the difficulty in fabricating such high aspect ratio (10:1 or higher) structures, ZPs fabricated by electron-beam lithography have been limited to a resolution of about 50 nm in the hard X-ray region (Nöhammer *et al.*, 2005). Recent improvements in fabrication technology will soon allow 30 nm or better to be reached (XRADIA; http://www.xradia.com/zpl_pd.htm) with commercially available devices. Increasing the aperture of these devices towards 1 mm is already possible. It should also be mentioned that diffractive optical elements with more complex functionality such as twin-spot zone plates (Di Fabrizio *et al.*, 2002) or computer-generated holograms *etc.* (Di Fabrizio *et al.*, 2003) can also be made. This unique feature can have interesting applications in the context of holography and other assisted phase-retrieval experiments. Multilayer-Laue ZPs offer the possibility of reaching a resolution beyond 10 nm with an efficiency greater than 30% (Kang *et al.*, 2006). Only one-dimensional focusing has been demonstrated so far by these devices; however, fabricating them with large zone aspect ratios is not difficult, thus they can have significant efficiency for hard X-rays.

One drawback of lithographic ZPs is that they are usually fabricated on thin transmitting substrates such as silicon nitride membranes, typically 100 nm in thickness. While these membranes only interact weakly with the incident beam, they have poor thermal conductivity. In addition, the heavy materials used to fabricate the zones, while thermally very stable, absorb a significant fraction of the incident beam. Consequently the lifetime of ZPs may turn out to be as short as a single X-ray pulse.

The possibility of combining the robustness of reflective optics with the diffraction-limited focusing of diffractive optics could be provided by using either multilayer-based or crystal-based Bragg–Fresnel lenses. They consist of a zone plate pattern etched into a reflecting surface. Although these elements are not used much at present, they can be made with small outermost zone width and large apertures (David & Souvorov, 1999). A disadvantage of Bragg–Fresnel lenses is that both the focus location and angle depend on the photon energy. Nonetheless, these devices may turn out to be an attractive alternative to presently considered solutions.

It is important to leave clear space around the sample, not least for the debris of used samples. For optics with apertures in the 1 mm range, the focal lengths will be larger than for the smaller optics used at present, which reduces the risk of damage. However, especially for extreme aperture angles, *i.e.* for high-resolution optics at long wavelengths, the working distances may be as small as a few centimeters. Compound optics is a promising approach, whereby apertures can be introduced in a number of places to clean up the beam. This may be required because of imperfections in the optics. An important question is whether or not to separate X and Y directions (as needed for KB mirror optics) or to retain cylindrical symmetry. Slits are easier than apertures to design and manipulate, so might be the preferred choice. The fact that such elements would need to be placed in the planes of an (intermediate) focus raises the issue of damage to the slit blades or apertures.

3.2. Stability and other experimental considerations

Many experiments can be carried out with the natural 0.08% bandwidth of the undulator because of the inherently small size of the diffracting object, but it will probably be worth having an optional Si(111) monochromator for the possible situations where the undulator is not up to specification or for large samples.

electronic reprint

All experiments will be in need of pulse-by-pulse diagnostics to determine photon flux, beam position and focus spot size at the sample position. Furthermore, it needs to be verified that the wavefront is stable in time. The spectral diagnostics should provide the mean photon energy and the content of higher harmonic radiation. Since it is anticipated that most experiments will be carried out by collecting data with single XFEL pulses, the stability requirements of the X-ray beam with respect to the sample are different compared with experiments at synchrotron sources. Beam pointing fluctuations and vibration will not lead to smearing of the spatial resolution, but will cause different locations on the sample to be illuminated. Precise reproducible positioning of the X-ray spot on the sample is therefore a further diagnostic requirement. Stabilization of the final focusing optics and sample can be handled to nanometer precision by optical interferometry.

In the experiments envisaged at the XFEL laboratory, the sample size of interest is envisaged to be below 1 μm. To collect diffraction data and to manipulate with extreme resolution such small samples, it will be necessary to set up high-resolution microscopes integrated to the diffractometer. This could be a present-day optical, SEM or AFM microscope that will be useful for identifying and aligning the sample on the diffractometer. The sample stage will need a single high-precision axis for tomography. Supporting samples on a membrane might work; if the membrane is blown away, the damage would be local and a second shot could be placed on an adjacent region. A square centimeter of sample will be enough for a million shots with 10 μm spacing.

Injection of a jet of liquid into the vacuum of the beamline is a method that should work but will severely limit the range of samples available. It might be possible to design a windowless flow cell in which a liquid is held in place by capillary forces. This might be made to work in a vacuum in some cases, but is certainly compatible with a helium environment. Levitated samples, either electrostatically, magnetically or by a gas stream, are another option. One should consider the option of not preparing individual particles at all. The particles could be blown through the X-ray beam in a highly diluted gas stream. This could be similar to the sample environment planned for the single molecule station. New techniques will have to be developed to synchronize the movement of such small particles with the X-ray beam and the detection system. One would obtain a series of diffraction patterns at random orientation of different particles, each recorded with a fully transversely coherent X-ray beam. Analytical techniques that have been established for electron diffraction will have to be applied here to analyze the diffraction patterns in order to obtain structural information about the samples. It will be advantageous to have a system for aligning particles in the focus of the beam at least in one direction, which will be an important factor for diffraction pattern sorting.

For most of the experiments proposed here, using windows around the sample in the focused beam should be avoided. The window material would become vaporized along with the sample. The use of windows could be possible for unfocused or attenuated beams but special care has to be taken regarding their quality. Possible restrictions could arise from the availability of X-ray windows. Ideally a beamline should be windowless so as not to interfere with the coherent wavefront. However, for practical reasons, thin windows could be used in the unfocused beam, before the optics, for example, or in the detector system. Silicon nitride membranes can be fabricated as thin as 50 nm, are radiation-hard, amorphous and contribute little undesired scattering (especially for hard X-rays). If kept to a size less than a few mm square, they can also support an air–vacuum interface such as a vacuum interface or a detector entrance window. Differential pumping could be viable, for example between a helium sample environment and the machine vacuum. This might be relatively easy to achieve, given the very large distances involved.

Since, for 12 keV radiation, windows can be allowed, user experiments could bring their own sample environment. Standard interchangeable sample environments (*e.g* baby chambers) should be provided in addition. For experiments at magnetic resonances (3–12 keV), in-vacuum magnet- and cryo-systems will be needed.

At 1 keV photon energy an instrument will differ from the 12 keV instrument in having a single vacuum system throughout, with no windows, including the detector chambers. A clever design of the vacuum system would allow plenty of in-vacuum motorized stages to mount optics at various distances. Perhaps there could be several sample stages at different distances from a fixed detector bank. Each one would have to have several translation stages packed close together to mount various optics. A good vacuum design needs to be flexible in allowing quick access for adjustments. Heating and cooling at the sample will be important as well as magnetic fields inside the vacuum.

Visible laser requirements will be similar to those imposed for pump–probe experiments. A distribution of visible laser radiation including the necessary synchronization and time-domain diagnostics should be included in the instrument design.

3.3. Detector and data acquisition requirements

It is envisaged that the different experimental stations would correspond to the different detector configurations. Since the whole experiment is a snapshot (or series of snapshots), there will be no use for diffractometers and single-point detectors. Only a complete diffraction pattern or complete image would be useful, so the detectors will be parallel, possibly massively parallel ($>10^9$ pixels). The detectors will have to be optimized for a given class of samples that would define the experimental station. Ideally the detectors should be able to distinguish each X-ray pulse of the XFEL. These experiments have high demands on two-dimensional X-ray detectors in terms of pixel number and pixel size.

There are certain requirements of a detector that have to be fulfilled in order that the CXDI technique can be successfully applied at XFEL. For a given particle size D, oversampling

electronic reprint

number s, wavelength λ and sample-to-detector distance L, the maximum pixel size p of the detector is given by

$$p = \frac{1}{s}\left(\frac{\lambda L}{D}\right).$$

For a maximum resolution R that can be obtained with a number of detector pixels N_D,

$$N_D = 2s(D/R).$$

From these two equations the size of the detector S_D is determined by

$$S_D = pN_D = 2(\lambda L/R).$$

From these simple equations one can easily estimate the pixel size and the total size of the detector for one's experiment. For example, if one wants to image a particle of size $D = 100$ nm in the forward-direction geometry at wavelength $\lambda = 0.1$ nm with sample-to-detector distance $L = 1$ m and sampling number $s = 5$, it will require a pixel size of the detector not bigger than $p = 200$ µm. For obtaining a resolution up to $R = 0.5$ nm, it will be necessary to have a detector of size 2K × 2K or 40 cm × 40 cm. If several Bragg peaks at different locations in reciprocal space have to be measured simultaneously, this would obviously increase the size of the detector. It is clear that realisation of such detectors will require a specific R&D effort.

There will be a wide bank of parallel detectors at a few meters distance to detect diffraction fringes from objects up to 10 µm in size (100 µm would be difficult). A sophisticated system of (conical) collimators in front of the detector bank is needed for a clean scattered signal.

Imaging experiments at fixed photon energy, *e.g.* at 12 keV, require a high-resolution in-line camera system to record the images. The detector format will need to be an array that is as large as possible (4K × 4K), optically coupled to an optimized fluorescent screen. The optical detector must be optimized for stability, linearity and reproducible background, but not so much for quantum efficiency.

One important consideration is the available computer power. On modern computers, three-dimensional fast Fourier transform calculations for 1024 × 1024 × 1024 data points can take about 10 s. Taking into account that, for the full reconstruction, several thousands of iterations will be needed, the time required for three-dimensional reconstruction of such a data set is ∼14 h at present. Such durations could become a serious limitation for operating with large data sets. The hope is that in the coming years the data storage and processing time will improve by several orders of magnitude, consistent with past trends in computational performance.

We should point out that development of the detector technology and data acquisition system is essential for the whole success of the described experiments. However, a more detailed discussion of these items is outside the scope of this article.

4. Realisation of a CXDI instrument at the European XFEL

The European XFEL facility will operate at energy 17.5 GeV [for technical details see Altarelli *et al.* (2006)]. The electron pulse will be distributed into two beamlines comprising three SASE FEL undulators and two undulators for ultrashort duration spontaneous synchrotron radiation. Two of the FEL undulators are designated for operation at an X-ray energy of 12.4 keV. One of them offers the possibility of photon energy variation by gap tuning. The third FEL undulator is designed for soft X-rays in the regime of 0.2 to 3.1 keV. Spontaneous radiation will be provided for the photon energy range of 20 to a few 100 keV. The radiation of the five undulators will be transported in long beamlines to the scientific instruments in the experiments hall. In the final state, ten dedicated instruments shall be operated. Owing to its high electron energy, the European XFEL is expected to reach a very high degree of spatial coherence at 12.4 keV (Saldin *et al.*, 2006). Compared with other FEL projects, the European XFEL is unique in its time structure of pulse repetition. Since the accelerator is superconducting, one can generate radio frequency pulses of duration ∼1 ms and with a repetition rate of 10 Hz. Within this pulse it is possible to accelerate up to 3000 electron bunches at a minimum spacing of 200 ns. Likewise, up to 30000 X-ray pulses per second can be produced and distributed to the various instruments.

The CXDI experiments can be divided into those requiring hard X-ray FEL radiation with energies up to 12 keV and those requiring soft X-rays up to 1 keV. Harder X-rays are requested in bulk investigations owing to penetration reasons. Another important reason for using hard X-rays is the fact that a kinematical approximation in the scattering on small samples can be safely used: multiple-scattering effects can be neglected making analysis of the scattering problem much easier. Therefore diffraction and imaging techniques will be applied at a photon energy of 12 keV. Investigation of magnetic systems will most probably use soft X-rays around 0.5–1.0 keV where the L edges of 3d transition metals in very thin samples can be used. Another application is the investigation of biological matter, preferably in the water window (0.28–0.5 keV) providing enhanced contrast between water and organic materials. An important biological application will be the study of initially living and hydrated biological objects, ideally *in vivo* (*e.g.* their natural environment). We propose further to use flash-frozen biological specimens maintained at cryogenic temperatures to minimize the observable effects of radiation damage. Another possibility is wet samples enclosed between very thin SiN membranes measured in transmission geometry. Photon energies around 1 keV can be used to investigate the structure and time evolution of non-organic nanostructures in the 20–50 nm range. For these particle sizes 1 keV radiation provides sufficient penetration but, in general, samples will not be isolated and will be surrounded by a vacuum. Otherwise they would be studied using electron microscopy. Instead we want to be able to access objects

electronic reprint

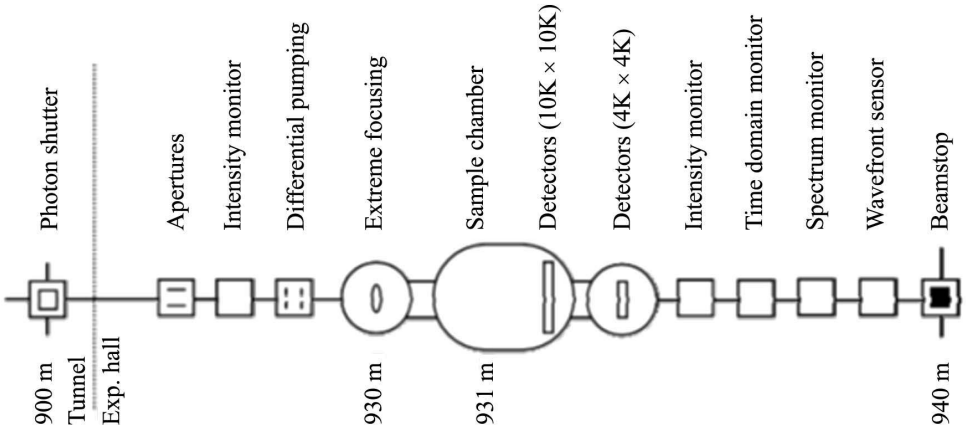

Figure 10
Schematic layout of a CXDI instrument at the SASE beamline at the XFEL Facility in Hamburg.

growing *in situ*, in contact with a liquid. We propose to use grazing-incidence small-angle scattering geometry, thus avoiding the penetration problem. In addition, energies in the soft X-ray range appear optimal for imaging of small biological specimens and comparing the estimated radiation damage *versus* resolution in electron microscopy, X-ray microscopy and X-ray crystallography data (Howells *et al.*, 2005). Since none of the European XFEL beamlines provide the entire photon energy range, more than one instrument is desirable for these types of experiments. A part of the materials science applications also requires for penetration purposes the use of very hard X-rays at energies 60–90 keV. These experiments will use the spontaneously emitted synchrotron radiation.

For diffraction experiments on crystals, the XFEL bandwidth of 8×10^{-4} is too large and monochromatization to $\Delta E/E \simeq 10^{-4}$ will be required. This requirement is similar to correlation experiments where one aims to increase the longitudinal coherence length. Diffraction experiments on non-crystalline matter, single particles and biomolecules can accept a much larger bandwidth. These experiments do not require additional monochromatization, but some require the maximum achievable photon flux at the sample, in particular those on single particles or molecules. Therefore two requirements exist and it is proposed to build the beam transport with the capability to use either double-crystal or double-mirror optics, both in a fixed-exit geometry. Following these optical elements, a collimator with a 10 mm hole is required to stop Bremsstrahlung radiation. Moderate focusing with a demagnification near unity requires placing focusing elements near the first optical elements. Compound refractive lenses, *e.g.* of Be, have the advantage of being in line and can be fast removed or inserted from the beam. They can further be used for both bandwidth options, although the effect of focal length variation owing to the chromaticity of the lens needs to be considered in the case of natural bandwidth ($\sim 10^{-3}$). For applications requiring the best possible preservation of wavefronts, *e.g.* in extreme focusing applications, no focusing will be used in the photon beam transport section and the lens is removed from the beam.

A schematic layout of a CXDI instrument is depicted in Fig. 10. Collimating apertures or a slit system will be placed in front of the experimental chamber for beam definition and to reduce scattered radiation from the X-ray beam. A gas photon flux monitor will follow before a differential pumping section separates the beamline from the UHV vacuum chamber for experiments. For hard X-rays, vacuum separation by means of Be or diamond windows are another possibility. Great care has to be taken on the perfection of these windows in order to preserve the wavefront properties. To achieve extreme focusing a special 0.1–1 µm focusing optics will be integrated into the instrument. In this case the upstream beamline optics will use only flat mirrors in order to minimize wavefront errors. In-line optics that can be switched in and out will be advantageous. The use of a pair of mirrors in KB geometry is another possibility. The optics is integrated in the sample environment system such that the distance between optics and sample can be fitted to the proper focal distance. The sample chamber should be equipped with a high-accuracy sample manipulator allowing *xyz* movements and rotation around two perpendicular axes. The chamber has to be capable of reaching 10^{-8} mbar for experiments requiring *in situ* sample preparation or being sensitive to surface contamination. Sample loading from external chambers needs to be foreseen. Diffraction in the forward direction should be collected by a large two-dimensional area detector. It will be required to vary the distance between sample and detector. Again Be windows could become useful if using He-filled flight paths.

The sample and its environment might absorb a significant fraction of the incident beam. It is, however, proposed to place most photon beam diagnostics in the transmitted beam. A second gas monitor detector will be used to measure the transmission. The spectral measurement should provide mean photon energy, bandwidth and higher harmonic content on a pulse-by-pulse basis. Measurement of the detailed spectral properties, *i.e.* the width and pulse shape, is performed only upon request. Diagnostics of time domain properties should deliver the arrival time required for pump–probe experiments using the visible laser. Finally, spatial measurements determine the beam location and its spatial distribution. Since these measurements are usually destructive they will be carried out in a dedicated set-up at the end of the line and before the beam stop.

In summary, we think that new XFEL sources will provide us with an exciting opportunity to probe nature at a subnano-

electronic reprint

meter resolution with femtosecond ultra-bright X-ray pulses. They will open for us new horizons in exploring the properties of condensed matter on these length and time scales.

Most of the material presented in this section is derived from the discussions in the working group 'Imaging, Phase Retrieval and Image Reconstruction' at the Workshop on Diffraction, Crystallography and Imaging at the European XFEL, which took place on 28 and 29 October 2005 at DESY. The authors are especially thankful to M. Altarelli, H. Dosch, J. Schneider and E. Weckert for careful reading and for their support during preparation of this manuscript.

References

Alexander, S. & McTague, J. P. (1978). *Phys. Rev. Lett.* **41**, 702–705.

Altarelli, M. *et al.* (2006). Editors. Report DESY 2006–097. DESY, Hamburg, Germany. (http://xfel.desy.de/tdr/index_eng.html.)

Arthur, J. *et al.* (2002). LCLS Conceptual Design Report. LCLS, USA. (http://www-ssrl.slac.stanford.edu/lcls/cdr/.)

Bartels, R. A., Paul, A., Green, H., Kapteyn, H. C., Murnane, M. M., Sterling Backus, S., Christov, I. P., Liu, Y., Attwood, D. & Jacobsen, C. (2002). *Science*, **297**, 376–378.

Bates, R. H. T. (1982). *Optik*, **61**, 247–262.

Bester, G., Nair, S. & Zunger, A. (2003). *Phys. Rev. B*, **67**, 161306.

Chao, W., Harteneck, B. D., Liddle, J. A., Anderson, E. H. & Attwood, D. T. (2005). *Nature (London)*, **435**, 1210–1213.

Chapman, H. N., Barty, A., Bogan, M. J. *et al.* (2006). *Nat. Phys.* **2**, 839–843.

Chapman, H. N., Barty, A., Marchesini, S., Noy, A., Cui, C., Howells, M. R., Rosen, R., He, H., Spence, J. C. H., Weierstall, U., Beetz, T., Jacobsen, C. & Shapiro, D. (2006). *J. Opt. Soc. Am.* A**23**, 1179–1200.

Cloetens, P., Ludwig, W., Baruchel, J., Van Dyck, D., Van Landuyt, J., Guigay, J. P. & Schlenker, M. (1999). *Appl. Phys. Lett.* **75**, 2912–2914.

Dagotto, E. (2005*a*). *Science*, **309**, 257–262.

Dagotto, E. (2005*b*). *New J. Phys.* **7**, 67.

David, C., Nöhammer, B. & Ziegler, E. (2001). *Appl. Phys. Lett.* **79**, 1088–1090.

David, C. & Souvorov, A. (1999). *Rev. Sci. Instrum.* **70**, 4168–4173.

Dawber, M., Rabe, K. M. & Scott, J. F. (2005). *Rev. Mod. Phys.* **77**, 1083–1130.

Di Fabrizio, E., Cojoc, D., Cabrini, S., Kaulich, B., Susini, J., Facci, P. & Wilhein, Th. (2003). *Opt. Express*, **11**, 2278–2288.

Di Fabrizio, E., Kaulich, B., Wilhein, T. & Susini, J. (2002). *Surf. Rev. Lett.* **9**, 243–248.

Di Fonzo, S., Jark, W., Lagomarsino, S., Giannini, C., de Caro, L., Cedola, A. & Müller, M. (2000). *Nature (London)*, **403**, 638–640.

Do, D.-H., Evans, P. G., Isaacs, E. D., Kim, D. M. & Eom, C. B. (2004). *Nat. Mater.* **3**, 365–369.

Eisebitt, S. (2007). Unpublished.

Eisebitt, S., Luning, J., Schlotter, W. F., Lorgen, M., Hellwig, O., Eberhardt, W. & Stohr, J. (2004). *Nature (London)*, **432**, 885–888.

Exarhos, G. J., Guenther, A. H., Kozlowski, M. R., Lewis, K. L. & Soileau, M. J. (1999). Editors. *Proceedings of the 30th Annual Conference on Laser Damage in Optical Materials*; *Proc. SPIE*, Vol. 3578.

Feil, M., Rubenchik, A. M., Kim, B.-M., da Silva, L. B. & Perry, M. D. (1998). *Appl. Surf. Sci.* **127–129**, 869.

Fienup, J. R. (1982). *Appl. Opt.* **21**, 2758–2769.

Finley, J. J., Sabathil, M., Vogl, P., Abstreiter, G., Oulton, R., Tartakovskii, A. I., Mowbray, D. J., Skolnick, M. S., Liew, S. L., Cullis, A. G. & Hopkinson, M. (2004). *Phys. Rev. B*, **70**, 201308(R).

Freund, H.-J., Bäumer, M., Libuda, J., Kuhlenbeck, H., Risse, T., Al-Shamery, K. & Hamann, H. (1998). *Cryst. Res. Technol.* **33**, 977–1008.

Jacobsen, C., Howells, M., Kirz, J. & Rothman, S. (1990). *J. Opt. Soc. Am.* A**7**, 1847–1861.

Jarre, A., Fuhse, C., Ollinger, C., Seeger, J., Tucoulou, R. & Salditt, T. (2005). *Phys. Rev. Lett.* **94**, 074801.

Jarre, A., Salditt, T., Panzner, T., Pietsch, U. & Pfeiffer, F. (2004). *Appl. Phys. Lett.* **85**, 161–163.

Hayden, H. W., Moffat, W. G. & Wulff, J. (1965). *Structure and Properties of Materials*, Vol. III. New York: Wiley.

Hayes, M. H. (1982). *IEEE Trans. Acoust. Speech Signal Process.* **30**, 140–154.

He, H., Weierstall, U., Spence, J. C. H., Howells, M., Padmore, H. A., Marchesini, S. & Chapman, H. N. (2004). *Appl. Phys. Lett.* **85**, 2454–2456.

Henderson, R. (1995). *Q. Rev. Biophys.* **28**, 171–193.

Hesse, A., Stangl, J., Holý, V., Roch, T., Bauer, G., Schmidt, O. G., Denker, U. & Struth, B. (2002). *Phys. Rev. B*, **66**, 085321.

Hignette, O., Cloetens, P., Morawe, Ch., Bernard, P. & Ludwig, W. (2006). *ESRF Highlights 2005*, pp. 108–109. ESREF, Grenoble, France.

Howells, M., Jacobsen, C., Kirz, J., Feder, R., McQuaid, K. & Rothman, R. (1987). *Science*, **238**, 514–517.

Howells, M. R., Beetz, T., Chapman, H. N., Cui, C., Holton, J. M., Jacobsen, C., Kirz, J., Lima, E., Marchesini, S., Miao, H., Sayre, D., Shapiro, D. A. & Spence, J. C. H. (2005). http://arxiv.org/abs/physics/0502059/.

Kang, H. C., Maser, J., Stephenson, G. B., Liu, C., Conley, R., Macrander, A. T. & Vogt, S. (2006). *Phys. Rev. Lett.* **96**, 127401.

Kegel, I., Metzger, T. H., Lorke, A., Peisl, J., Stangl, J., Bauer, G., Nordlund, K., Schoenfeld, W. V. & Petroff, P. M. (2001). *Phys. Rev. B*, **63**, 035318.

Klein, W. (2001). *Phys. Rev. E*, **64**, 056110.

Larson, B. C., Yang, W., Ice, G. E., Budai, J. D. & Tischler, J. Z. (2002). *Nature (London)*, **415**, 887–890.

Lindaas, S., Howells, M., Jacobsen, C. & Kalinovsky, A. (1996). *J. Opt. Soc. Am.* A**13**, 1788–1800.

McNulty, I., Kirz, J., Jacobsen, C., Anderson, E. H., Howells, M. R. & Kern, D. P. (1992). *Science*, **256**, 1009–1012.

Malachias, A., Kycia, S., Medeiros-Ribeiro, G., Magalhães-Paniago, R., Kamins, T. I. & Williams, R. S. (2003). *Phys. Rev. Lett.* **91**, 176101.

Malachias, A., Schülli, T. U., Medeiros-Ribeiro, G., Cançado, L. G., Stoffel, M., Schmidt, O. G., Metzger, T. H. & Magalhães-Paniago, R. (2005). *Phys. Rev. B*, **72**, 165315.

Mecke, K. (2007). Personal communication.

Miao, J., Charalambous, P., Kirz, J. & Sayre, D. (1999). *Nature (London)*, **400**, 342–344.

Miao, J., Chen, C.-C., Song, C., Nishino, Y., Kohmura, Y., Ishikawa, T., Ramunno-Johnson, D., Lee, T.-K. & Risbud, S. H. (2006). *Phys. Rev. Lett.* **97**, 215503.

Miao, J., Ishikawa, T., Johnson, B., Anderson, E. H., Lai, B. & Hodgson, K. O. (2002). *Phys. Rev. Lett.* **89**, 088303.

Mimura, H., Matsuyama, S., Yumoto, H., Hara, H., Yamamura, K., Sano, Y., Endo, K., Mori, Y., Yabashi, M., Nishino, Y., Tamasaku, K., Ishikawa, T. & Yamauchi, K. (2006). *Proceedings of the 8th International Conference on X-ray Microscopy, IPAP Conference Series 7*, pp. 100–102.

Narvaez, G. A., Bester, G. & Zunger, A. (2005). *Phys. Rev. B*, **72**, 245318.

Neev, J., Da Silva, L. B., Feit, M. D., Perry, M. D., Rubenchik, A. M. & Stuart, B. C. (1996). *IEEE J. Quantum Electron.* **2**, 790–800.

Nöhammer, B., David, C., Burghammer, M. & Riekel, C. (2005). *Appl. Phys. Lett.* **86**, 161804.

Nöhammer, B., Hoszowska, J., Freund, A. K. & David, C. (2003). *J. Synchrotron Rad.* **10**, 168–171.

Nosé, S. & Yonezawa, F. (1986). *J. Chem. Phys.* **84**, 1803–1814.

electronic reprint

Nugent, K. A., Peele, A. G., Chapman, H. N. & Mancuso, A. P. (2003). *Phys. Rev. Lett.* **91**, 203902.
Perry, M. D., Stuart, B. C., Banks, P. S., Feit, M. D., Yanovsky, V. & Rubenchik, A. M. (1999). *J. Appl. Phys.* **85**, 6803–6810.
Pfeifer, M. A., Williams, G. J., Vartanyants, I. A., Harder, R. & Robinson, I. K. (2006). *Nature (London)*, **442**, 63–66.
Pfeiffer, F., David, C., Burghammer, M., Riekel, C. & Salditt, T. (2002). *Science*, **297**, 230–234.
Pfeiffer, F., David, C., van der Veen, J. F. & Bergemann, C. (2006). *Phys. Rev. B*, **73**, 245331.
Plech, A., Kotaidis, V., Lorenc, M. & Boneberg, J. (2006). *Nat. Phys.* **2**, 44–47.
Poulsen, H. F. (2004). *Three-Dimensional X-ray Diffraction Microscopy*. Berlin: Springer.
Quiney, H. M., Peele, A. G., Cai, Z., Paterson, D. & Nugent, K. A. (2006). *Nat. Phys.* **2**, 101–104.
Riedel, H. (1992). *Fracture Mechanisms*, in *Materials Science and Technology*, Vol. 6, edited by R. W. Cahn, P. Haasen and E. J. Kramer. Weinheim: VCH.
Robinson, I. K., Libbert, J. L., Vartanyants, I. A., Pitney, J. A., Smilgies, D. M., Abernathy, D. L. & Grübel, G. (1999). *Phys. Rev. B*, **60**, 9965–9972.
Robinson, I. K., Vartanyants, I. A., Williams, G. J., Pfeifer, M. A. & Pitney, J. A. (2001). *Phys. Rev. Lett.* **87**, 195505.
Rosenfeld, G., Becker, A. F., Poelsema, B., Verheij, L. K. & Comsa, G. (1992). *Phys. Rev. Lett.* **69**, 917–920.
Rouhi, M. (1999). *Chem. Eng. News*, **77**(46), 8–9.
Saldin, E. L., Schneidmiller, E. A. & Yurkov, M. V. (2006). DESY Preprint 06–137. DESY, Hamburg, Germany.
Sayre, D. (1952). *Acta Cryst.* **5**, 843.
Schroer, C. G. (2006). *Phys. Rev. B*, **74**, 033405.
Schroer, C. G., Kuhlmann, M., Hunger, U. T., Günzler, T. F., Kurapova, O., Feste, S., Frehse, F., Lengeler, B., Drakopoulos, M., Somogyi, A., Simionovici, A. S., Snigirev, A., Snigireva, I., Schug, C. & Schröder, W. H. (2003). *Appl. Phys. Lett.* **82**, 1485–1487.
Schroer, C. G., Kurapova, O., Patommel, J., Boye, P., Feldkamp, J., Lengeler, B., Burghammer, M., Riekel, C., Vincze, L., van der Hart, A. & Küchler, M. (2005). *Appl. Phys. Lett.* **87**, 124103.
Schroer, C. G. & Lengeler, B. (2005). *Phys. Rev. Lett.* **94**, 054802.
Schülli, T. U., Stangl, J., Zhong, Z., Lechner, R. T., Sztucki, M., Metzger, T. H. & Bauer, G. (2003). *Phys. Rev. Lett.* **90**, 066105.
Shen, Y. C. & Oxtoby, D. W. (1996). *Phys. Rev. Lett.* **77**, 3585–3588.
Shpyrko, O. G., Isaacs, E. D., Logan, J. M., Feng, Y., Aeppli, G., Jaramillo, R., Kim, H. C., Rosenbaum, T. F., Zschack, P., Sprung, M. & Sandy, A. R. (2007). *Nature (London)*, **447**, 68–71.
Siders, C. W., Cavalleri, A., Sokolowski-Tinten, K., Tóth, Cs., Guo, T., Kammler, M., Horn von Hoegen, M., Wilson, K. R., von der Linde, D. & Barty, C. P. J. (1999). *Science*, **286**, 1340–1342.
Stangl, J., Hesse, A., Holý, V., Zhong, Z., Bauer, G., Denker, U. & Schmidt, O. G. (2003). *Appl. Phys. Lett.* **82**, 2251–2253.
Stangl, J., Holý, V. & Bauer, G. (2004). *Rev. Mod. Phys.* **76**, 725–783.
Stuart, B. C., Feit, M. D., Herman, S., Rubenchik, A. M., Shore, B. W. & Perry, M. D. (1996*a*). *Phys. Rev. B*, **53**, 1749–1761.
Stuart, B. C., Feit, M. D., Herman, S., Rubenchik, A. M., Shore, B. W. & Perry, M. D. (1996*b*). *J. Opt. Soc. Am.* B**13**, 459–468.
Stuart, B. C., Feit, M. D., Rubenchik, A. M., Shore, B. W. & Perry, M. D. (1995). *Phys. Rev. Lett.* **74**, 2248–2251.
Tanaka, T. & Shintake, T. (2005). *SCSS X-FEL Conceptual Design Report*, edited by Takashi Tanaka and Tsumoru Shintake. SCSS XFEL, R&D Group, RIKEN Harima Institute/SPring-8, Japan. (http://www-xfel.spring8.or.jp/SCSSCDR.pdf.)
Trebes, J. E., Brown, S. B., Campbell, E. M., Matthews, D. L., Nilson, D. G., Stone, G. F. & Whelan, D. A. (1987). *Science*, **238**, 517–519.
Vartanyants, I. A. & Robinson, I. K. (2001). *J. Phys. Condens. Matter*, **13**, 10593–10611.
Vartanyants, I. A. & Robinson, I. K. (2003). *J. Synchrotron Rad.* **10**, 409–415.
Vartanyants, I. A., Robinson, I. K., Onken, J. D., Pfeifer, M. A., Williams, G. J., Pfeiffer, F., Metzger, H., Zhong, Z. & Bauer, G. (2005). *Phys. Rev. B*, **71**, 245302.
Weitkamp, T., Nöhammer, T. B., Diaz, A., David, C. & Ziegler, E. (2005). *Appl. Phys. Lett.* **86**, 054101.
Weitkamp, T., Patommel, J., Schroer, C. *et al.* (2007). In preparation.
Wiebach, Th., Schmidbauer, M. M., Hanke, M. M., Raidt, H., Köhler, R. & Wawra, H. (2000). *Phys. Rev. B*, **61**, 5571–5578.
Williams, G. J., Pfeifer, M. A., Vartanyants, I. A. & Robinson, I. K. (2003). *Phys Rev. Lett.* **90**, 175501.
Williams, G. J., Pfeifer, M. A., Vartanyants, I. A. & Robinson, I. K. (2006). *Phys. Rev. B*, **73**, 094112.
Williams, G. J., Quiney, H. M., Dhal, B. B., Tran, C. Q., Nugent, K. A., Peele, A. G., Paterson, D. & de Jonge, M. D. (2006). *Phys. Rev. Lett.* **97**, 025506.
Xiao, X. & Shen, Q. (2005). *Phys. Rev. B*, **72**, 033103.

electronic reprint